Available online at www.sciencedirect.com
SCIENCE DIRECT®
Journal of Organometallic Chemistry 685 (2003) 122–133
Journal of Organometallic Chemistry
www.elsevier.com/locate/jorganchem

Mini review

Optical properties of polysilanes with various silicon skeletons

Akira Watanabe *

Institute of Multidisciplinary Research for Advanced Materials, Tohoku University, Katahira, Aoba-ku, Sendai 980-8577, Japan

Received 23 January 2003; accepted 17 March 2003

Abstract

In this account, I present a brief overview of the optical properties of polysilanes with various silicon skeletons reviewing previous studies and supplying new experimental results. The optical properties of branched polysilanes such as network polysilane (polysilyne), polysilane dendrimer, and organosilicon nanocluster (OSI) are discussed here. These polysilanes have higher dimensionalities in comparison with a linear polysilane that can be considered as a one-dimensional silicon. The optical properties of the polysilanes are remarkably influenced by the structure of the silicon skeleton. The emission spectra of branched polysilanes are characterized by the dual emission in the UV and visible regions and the large Stokes shift between the absorption and emission spectra. The dual emission was explained by a configuration coordinate model considering the emissions from the excited state of the linear Si–Si chain and a localized excited state of branching points. The localized excited state induced by the distortion of the Si–Si chain around the branching point was suggested. The time-resolved emission spectra of polysilane dendrimer show the energy migration from the linear Si–Si chain to the branching point. The quantum size effect also influences the optical properties of polysilanes. The optical energy gap of OSI decreased remarkably with increasing the size. Further decrease of the energy gap was observed by heat treatment of the OSI film, which was explained by the reconstruction of the Si skeleton accompanying the elimination of organic side chain.

Keywords: Polysilane; Network polysilane; Branched polysilane; Polysilane dendrimer; Optical property; Emission; Excited state; Quantum size effect

1. Introduction

Polysilane (polysilylene) consisting of a Si–Si main chain and organic side chains has received considerable attention due to the emission in the UV-visible region, which is a feature different from inorganic silicons [1,2]. The linear Si–Si chain of a polysilane can be considered to be a pseudo-one-dimensional silicon chain when compared with a three-dimensional crystalline silicon (*c*-Si) [2]. One of the expectations for the study on polysilane is that we can bridge the interdisciplinary field between one-dimensional and three-dimensional silicons with polysilanes having various Si-skeletons. The advantage of organic silicons is the flexibility in the molecular design and synthesis. The emission properties of polysilanes with various Si-skeletons provide important information on the relationship between the Si dimensionality and physical properties. Polysilanes with various kinds of silicon skeletons have been reported in the last decade, for example, branched polysilane [poly(silylene-co-silyne)] [3,4], network polysilane (polysilyne) [5–10], ladder polysilane [11], organosilicon nanocluster (OSI) [12–14], polysilane dendrimer [15–17,31–34], etc. The network polysilane is synthesized by the reaction of trichloroorganosilane, and the branched polysilane prepared by the copolymerization of the dichloro- and trichloro-organosilanes has an intermediate structure between the linear and network polysilanes. The ratio of the branched Si–Si chain to the linear Si–Si chain can be varied by the feed composition of the monomers [4]. As a three-dimensionally branched polysilane, an organosilicon monocluster (OSI) was prepared from tetrachlorosilane. The OSI has a hyperbranched structure involving a four-coordinate silicon atom [12]. Fig. 1 shows the classification of polysilanes based on the Si-dimensionalities, where only Si chains are illustrated schematically. In this paper, I present a

* Fax: +81-22-217-5659.
E-mail address: watanabe@tagen.tohoku.ac.jp (A. Watanabe).

0022-328X/03/$ - see front matter © 2003 Elsevier B.V. All rights reserved.
doi:10.1016/S0022-328X(03)00649-1

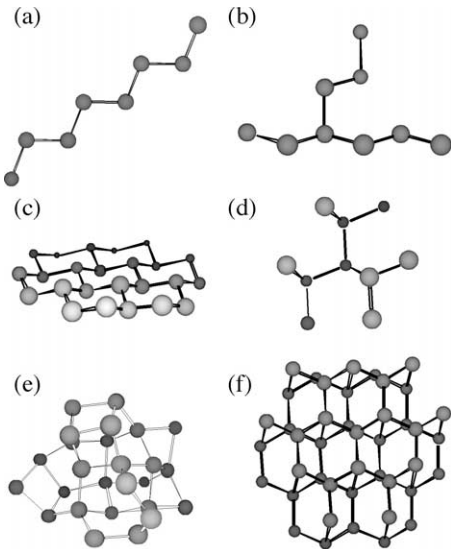

Fig. 1. Classification of polysilanes based on the Si-dimensionalities. (a) Linear polysilane (polysilylene), (b) branched polysilane, (c) network polysilane (polysilyne), (d) polysilane dendrimer, (e) organosilicon nanocluster (OSI), (f) silicon nanocrystal.

brief overview of the optical properties of polysilanes with various dimensionalities reviewing previous studies and supplying new experimental results. The information of the optical properties of the organic Si chain may contribute to understanding the visible emission properties of inorganic silicon such as porous silicon. The emission properties of silicon with a low-dimensional structure are a topic of great interest. In the field of inorganic silicon, the visible emission from porous silicon has been an exciting research area for the past decade [18–21]. The properties of a visible light emission from porous silicon are significantly different from those of crystalline silicon (*c*-Si) and amorphous silicon (*a*-Si), which show no emission at room temperature and very weak emission at low temperature in the near-IR region, respectively [22]. Silicon is the main semiconductor in the electronics industry, but one drawback of silicon is its nonemissive property. The visible emission from porous silicon was explained by the quantum confinement effect of the column-like structure with a nanometer size [18]. Later, the oxidized structure on the silicon surface, which is called siloxene, was suggested as another reason for the visible emission [23,24]. However, the origin of the visible emission has not yet been clarified, because the oxidized surface structure of porous silicon is not homogeneous and cannot be adequately characterized.

2. Synthesis and characterization of polysilanes with various silicon skeletons

The most common procedure to prepare a linear polysilane is the condensation of dichlorodiorganosilane by the Kipping reaction using a sodium metal in toluene at 110 °C with rapid stirring. The molecular weight distribution of linear poly(methylphenylsilylene) becomes narrow by the addition of crown ether [25]. Polysilyne having a silicon network structure was prepared by similar procedures using trichloroorganosilane as a monomer. Branched polysilanes were prepared by copolymerization of dichlorodiorganosilane and trichloroorganosilane. These reactions are depicted in Fig. 2 schematically. The network polysilane was recognized as a polymer that has a two-dimensional Si-skeleton as depicted by Fig. 1 and a two dimensional σ-conjugation along the Si-skeletons in the beginning stage. Watanabe et al. investigated the Si-skeleton of network polysilanes using far-IR spectroscopy [9,10]. By comparison of the far-IR spectra and calculated vibrational spectra for silicon model compounds, it was suggested that the silicon skeleton of network polysilane consists of various kinds of silicon rings, such as 4-, 5-, and 6-membered rings. By analogy to the linear and network polysilanes, the synthesis of a three dimensional polysilane can be expected by the reaction of tetrachlorosilane as a monomer. Watanabe et al. have reported the synthesis of the three-dimensional polysilane by the reaction of tetrachlorosilane using Mg metal in tetrahydrofuran (THF) and the capping reaction of the remaining Si–Cl group by an alkyl Grignard reagent at the end of the reaction [12–14]. In the reaction, the dispersed silicon cluster in THF solution is solubilized by the substitution of the Cl group of the cluster fringe with an organic group. The Si cluster solubilized by organic substituents is nanometer size, therefore, it was named organosilicon nanocluster (OSI). The rather mild conditions of the polysilane synthesis is advantageous compared to the usual Kipping reaction using a fused

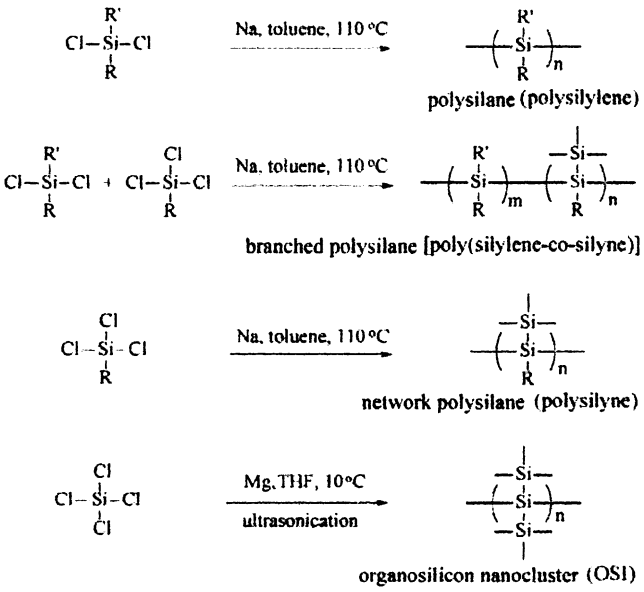

Fig. 2. Synthesis of polysilanes with various Si skeleton.

sodium metal in a hot toluene. However, the crude OSI contains the oxidized components and inorganic impurities come from Mg metal, therefore, the crude products were purified by column chromatography using silica gel and non-polar *n*-hexane as the eluent. Fig. 3 shows the FT-IR spectra of *n*-propyl-substituted OSI before and after column chromatography. Before column chromatography, the intense signals attributed to Si–OH, Si–H, and Si–O–Si are observed around 3400, 2100, and 1000 cm^{-1}, respectively, in Fig. 3 (a). These signals are completely disappeared after column chromatography, as shown in Fig. 3 (b). Based on the elemental analysis, the composition of the OSI was determined to be $Si(n\text{-}C_3H_7)_{0.64}$. The molecular weight, M_w, and the distribution (M_w/M_n, M_w: weight-average molecular weight; M_n: number-average molecular weight) of the organosilicon cluster were determined to be 2080 and 1.16, respectively, by gel permeation chromatography (GPC) using the THF eluent and monodispersed polystyrenes as the standards. From the elemental analysis and the GPC, the number of Si atoms in an OSI molecule is estimated to be about 30. The percentages of the three kinds of Si atoms, i.e., four-, three-, and two-coordinate silicon atoms, can be estimated from the cross polarization magic angle spinning (CPMAS) ^{29}Si-NMR spectrum of the OSI [12]. By the curve fitting of the ^{29}Si-NMR spectrum, the percentages of four-, three-, and two-coordinate silicon atoms can be estimated to be 32, 13, and 55%, respectively. The Si skeleton of the OSI is amorphous because the OSI shows a broad Raman band assigned to the transverse optical (TO)–phonon band [26,27]. Fig. 4 shows one of the possible structures of OSI molecule. Although the exact structure of the amorphous Si skeleton cannot be determined, the molecular model gives the image of the Si cluster surrounded by *n*-propyl groups, which causes the solubility in common organic solvents.

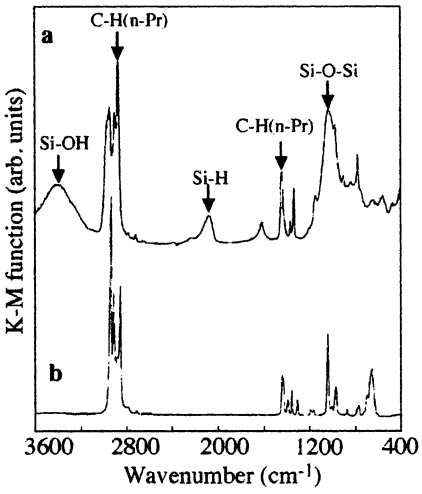

Fig. 3. FT-IR spectra of *n*-propyl-substituted OSI before purification by column (a) and after purification by column.

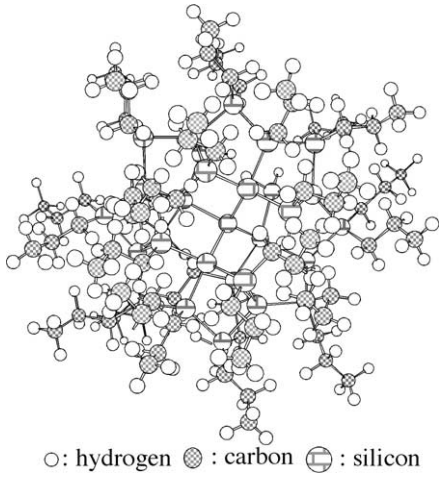

Fig. 4. The image of the molecular structure of OSI.

Polysilane dendrimers are also three-dimensional polysilanes [15–17,28–31]. Polysilane dendrimers that have regular branching Si–Si chains are an ideal model for the branched polysilanes. Recently, the excited dynamics of polysilane dendrimers with various sizes (0-, 1-, and 2-generation) have been reported by Sekiguchi et al. [30,31].

3. Absorption and emission spectra of branched polysilanes

The electronic state of the linear polysilane (polysilylene) is characterized by the σ-conjugation which is caused by overlapping of the Si $3sp^3$ orbitals along the Si–Si chain. The absorption and emission spectra of polysilane changed dramatically with branching structure. In Figs. 5 and 6, the absorption and emission spectra of linear, branched, and network polysilanes are compared [4]. The branched polysilanes were synthesized by the copolymerization of dichloromethylphenylsilane and trichlorophenylsilane varying the ratio. In Figs. 5 and 6, the polysilanes are represented by PMePhSi D/T using the monomer feed composition ratio of dichloromethylphenylsilane to trichlorophenylsilane (D/T). The polymer composition was determined by ^{1}H-NMR on the basis of the signals of methyl proton and phenyl proton. The ratios of methylphenylsilylene unit to phenyl unit correspond well to those of monomer feed composition. Linear poly(methylphenylsilylene) (PMePhSi 10/0) shows a sharp σ–σ* absorption band at 334 nm as shown in Fig. 5. The absorption at 273 nm is attributable to π–π* band of the phenyl group. The absorbance of the σ–σ* band decreases and the absorption at 250 nm increases with increasing the

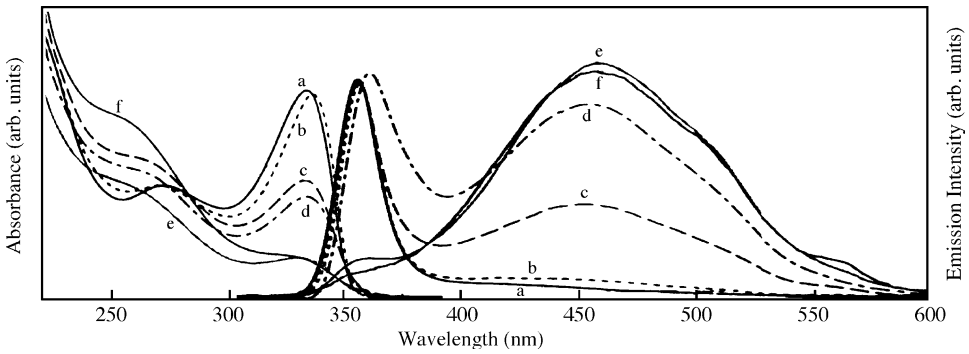

Fig. 5. Absorption and emission spectra of poly(methylphenylsilylene co-phenylsilyne)s in THF. (a) PMePhSi 10/0, (b) PMePhSi 9/1, (c) PMePhSi 8/2, (d) PMePhSi 7/3, (e) PMePhSi 6/4, (f) PMePhSi 5/5. Concentration; 8×10^{-4} M (Si unit).

feed composition of trichlorophenylsilane. Such a tendency becomes more clear for PMePh D/T with high trichlorophenylsilane composition as shown in Fig. 6. The absorption at 330 nm almost disappears and the absorption edge shifts to longer wavelength. Poly(phenylsilyne) (PMePhSi 0/10) shows an absorption edge at 410 nm.

The emission spectra of polysilanes were also influenced dramatically by the branching structure. In Fig. 5, emission spectrum of poly(methylphenylsilylene) (PMePhSi 10/0) shows a sharp emission peak, exhibiting the mirror image with σ–σ^* absorption band. Such an emission spectrum is assigned to a linear Si–Si chain of polysilane. With increasing the trichlorophenylsilane component in monomer feed composition, a broad emission appears at 450 nm. Polysilanes with a high trichlorophenylsilane feed composition show only a broad emission (Fig. 6). The emission spectra were obtained by the excitation at 280 nm. The shapes of the emission spectra were independent of excitation wavelength.

Considering the relationship between absorption and emission spectra, a linear polysilane shows sharp absorption and emission bands in the UV region indicating a mirror image, where the transition energies of the absorption and emission are similar and their spectral shapes are symmetrical. This result indicates that the geometries at the potential minima in the ground and excited states are similar. The red shift of absorption suggests the extent of the σ-conjugation with increasing dimensionality of the Si skeleton. The visible emission properties of the network polysilanes are characterized by the broadness and a large Stokes shift. For the branched polysilane, with the increasing branching structure, a continuous increase in the σ-conjugation and the continuous red shift of the emission spectrum were expected. However, the branched polysilane showed two kinds of emission maxima at around 360 and 460 nm, and the ratio is changed depending on the branching structure [4]. The former is a sharp one and assigned to the emission from the linear Si–Si chain. The latter is a broad one which is analogous to a network polysilane. Similar broad emission has been also observed for OSI which has a hyperbranched structure involving a four-coordinate silicon atom [13,35]. Surprisingly, a cyclic silicon compound, octaphenyltetracyclosilane, which has no branching point, also shows a similar broad visible emission as reported in the previous paper [35]. These results suggest a common structure in the excited state, which does not depend on the Si–Si chain size and structure. This problem will be discussed in detail in Section 4.

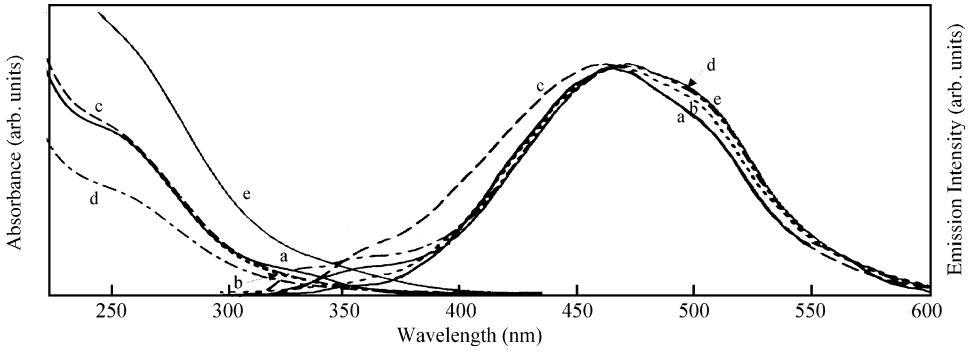

Fig. 6. Absorption and emission spectra of spectra of poly(methylphenylsilylene co-phenylsilyne)s in THF. (a) PMePhSi 4/6, (b) PMePhSi 3/7, (c) PMePhSi 2/8, (d) PMePhSi 1/9, (e) PMePhSi 0/10. Concentration; 8×10^{-4} M (Si unit).

4. Excited states of branched polysilanes

The visible broad emission from polysilanes has been related to the branching point of the Si–Si chain [33]. However, the assignment of the excited structure around the branching point is difficult because these polysilanes do not have a regular structure. The inhomogeneity of the Si–Si chain causes the complicated kinetics of the emission processes and analysis of the polydispersed emission kinetics has many difficulties and obscurities. In contrast, a polysilane dendrimer has regular branching Si–Si chains [15–17,28–31], and it is an ideal model for the branched polysilanes. Sekiguchi et al. have reported the synthesis of polysilane dendrimers as shown in Fig. 7 [16,30,31]. **1G** is a first-generation dendrimer that has four branching points. **2G** is a second-generation dendrimer that has ten branching points. **0G** corresponds to the basic branching unit of the polysilane dendrimers. The polysilane dendrimers **0G**, **1G**, and **2G** shows absorption maxima at 242, 269, and 279 nm, respectively. Sekiguchi et al. have reported the excited state dynamics of these polysilane dendrimers by time-resolved emission spectroscopy to reveal the origin of the broad visible emission from the branched Si–Si chain [34]. The time-resolved emission spectra for **1G** in a rigid 3-methylpentane matrix at 77 K are shown in Fig. 8 [34]. In the measurements, the emissions of the dendrimers were observed in a dilute solution where intermolecular interaction and energy transfer between dendrimer molecules are negligible, because we wished to focus our attention on the intramolecular dynamics of the excited state. The remarkable feature in Fig. 8 is the spectral change upon increasing the delay time after laser excitation. At the early stage within 20 ns, UV emission around 350 nm is observed, which is indicated by the arrow in Fig. 8

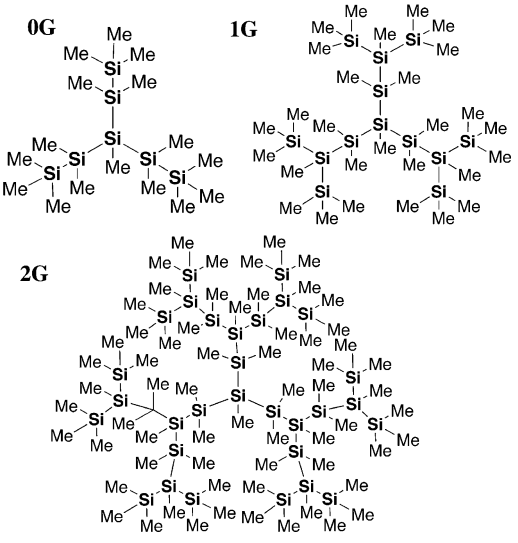

Fig. 7. Structural formulas of polysilane dendrimers and the abbreviations.

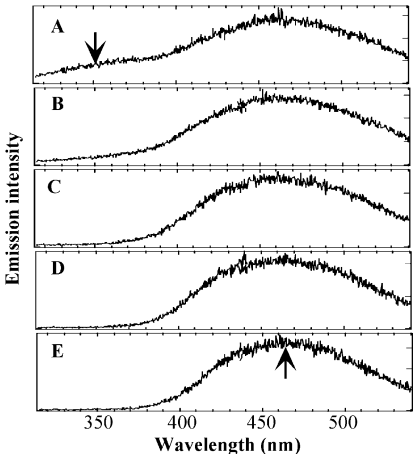

Fig. 8. Time-resolved emission spectra of 1G in 3-methylpentane at 77 K: (A) 0–2 ns, (B) 2–4 ns, (C) 5–7 ns, (D) 10–12 ns, (E) 20–22 ns. Excitation wavelength: 279 nm.

(A). This UV emission can be attributed to that from a linear part of the Si–Si chain. On increasing the delay time, the relative intensity of the UV emission decreases in comparison with a broad emission in the visible region around 460 nm. The dendrimer 0G and 2G also show similar features [34]. The polysilane dendrimers also show the large Stokes shift between absorption and visible emission spectra. These features are also similar to those of network polysilanes. That is, the emission spectra of branched polysilanes are characterized by the dual emission in the UV and visible regions and the large Stokes shift.

The dual emission properties of the polysilane dendrimer were attributed to the two kinds of emissive points, such as linear and branching parts of the Si–Si chain. The intramolecular energy transfer (energy migration) from the linear to branched part was suggested by the time profiles for the emission of **1G** in 3-methylpentane at 77 K monitored at 350 and 460 nm [34]. The emission decay of **1G** monitored at 350 nm showed a single-exponential decay curve. The single-exponential decay curve is reasonable behavior for an isolated molecule located in a dilute solution. On the other hand, the time-profile monitored at 460 nm clearly showed the growth of the emission intensity upon increasing the delay time. The growth is attributable to intramolecular energy transfer because the concentration of the sample solution is below 5×10^{-5} M and it is dilute enough to inhibit intermolecular energy transfer. It is surprising that dual emission in the UV and visible regions was observed even for the small dendrimer. This may be due to the small energy gap between the two kinds of excited states and random hopping between them.

The above results can be explained by considering a configuration coordinate model depicted in Fig. 9. The large Stokes shift is explained by the different minimum

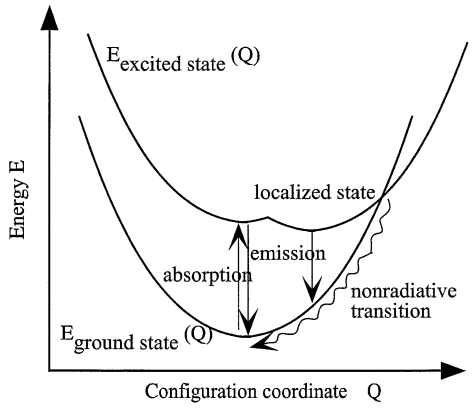

Fig. 9. Configuration coordinate model for polysilane dendrimer.

energy points along the configuration coordinate. After photoexcitation, a localized excited state is generated by distortion of the molecules in the excited state. The population of the energy levels on the potential curve in the excited state can be expressed by the Gaussian distribution curve. The broadness of the emission spectrum is caused by the thermal distribution of the energy levels in the excited state and the transition to the curvature of the potential curve in the ground state. In the case of the polysilane dendrimer, the dual emission in the UV and visible regions suggests the existence of two kinds of excited states on the potential curve. Another feature of the configuration coordinate model is deactivation of the excited state via the crossing point between potential curves for the ground and excited states. The non-radiative transition reduces the emission quantum efficiency. In fact, the quantum efficiency of the broad visible emission of a network polysilane is 0.001 while the linear polysilane with a small Stokes shift shows a quantum efficiency higher than 0.1.34 [35]. The quantum efficiency of the polysilane dendrimer is also not high, that of **1G** was determined to be 0.014, which is due to the nonradiative transition as depicted in Fig. 9.

The geometrical distortion of the Si–Si chain in the excited state was estimated by semiempirical MO calculations for the ground and excited states [35]. Fig. 10 shows the conformations of **0G** in the ground and excited states by semiempirical MO calculations using the geometries of Si and C atoms except H are depicted. The initial geometry was constructed based on the crystalline structure of the polysilane dendrimer, and then the conformation was optimized by the MO calculation. In comparison with conformation **A** in the ground state, conformation **B** in the excited state shows changes of the bond angles. The remarkable feature of conformation **B** in the excited state is the unusual bond angle of 60° for the Si1–Si4–Si5 sequence. Overlap of the electron cloud and an interaction between Si1 and Si5 were suggested by the MO calculation in the excited state. The bond order between Si1 and Si5 increased from 0.005 in the ground state to 0.047 in the excited state. Therefore, the Si1, Si4, and Si5 atoms form a structure similar to the Si 3-membered ring in the excited state. The visible emission can be attributed to that from the localized excited state that is induced by the distortion of the Si–Si chain around the branching point in the excited state. On the other hand, the MO calculations for a linear Si–Si chain did not show such a serious distortion in the excited state. In the case of a homogeneous Si–Si chain of the linear polysilane, the extension of the σ-electron cloud along the linear Si–Si chain works as a buffer for the distortion which is induced by the difference of the electron distribution between the ground and excited states. In contrast to this, in the case of the branched polysilane, the distortion is focused on the branching points, and the σ-conjugation is discontinued at these points, forming the localized excited state having a triangle structure as shown in Fig. 10 B. The behavior is analogous to that of a self-trapped exciton. In Fig. 10 B, the increase of the bond angle for the Si6–Si1–Si4 sequence must be caused by steric hindrance of the S6 atom and the methyl groups.

The time-resolved emission spectra of *n*-propyl-substituted OSI film at 6.0 K are shown in Fig. 11. The

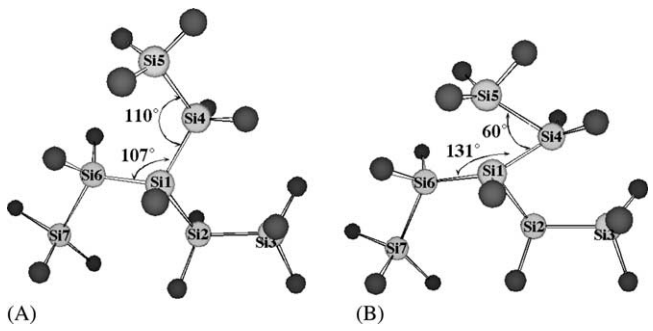

Fig. 10. Conformations of ground and excited states of **0G** by semiempirical MO calculations using PM3 method: (A) ground state; (B) excited state.

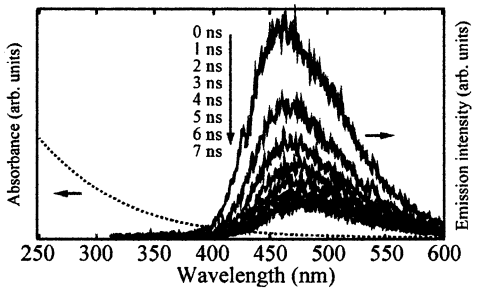

Fig. 11. Time-resolved emission spectra of *n*-propyl-substituted-OSI film at 6 K. Excitation wavelength: 240 nm. The time-resolved spectrum at 0 ns shows the accumulated one from 0 ns to 1 ns. The accumulated width is 1 ns and the starting time is indicated in the figure as a delay time. Dotted line is the absorption spectrum of OSI film.

emission maximum and the broad shape of the emission spectra for OSI consisting of four-coordinate silicon atom are similar to those of network polysilanes and polysilane dendrimers with a three-coordinate silicon atom. In Fig. 11, the emission maximum shifts to longer wavelengths with the increasing delay time after the laser-pulse excitation. The emission maximum at 461 nm for the spectrum at 0 ns shifts to 479 nm for that at 7 ns. Such a peak shift can be explained by considering the migration of the excited state to a defect at the lower energy levels because the silicon network structure is amorphous and the σ-conjugation state depends on the conformation of the Si-skeleton. Such an energy migration from the higher to the lower energy defect is caused by the random structure of the Si chain. In solid phase, the intermolecular energy transfer between OSI molecules also contributes to the shift of emission maximum.

5. Size effects in the optical properties

In the above sections, the effects of the Si branching structure on the optical properties of polysilanes were discussed. Recently, the visible emission from porous silicon is one of the exciting problems and the origin of the visible emission has been discussed in relation to the quantum size effect of the nanostructure [18–21]. The sizes of the polysilanes are just nanometer, and the quantum size effect should also be considered in the optical properties. In the field of inorganic silicon, some models were proposed for the visible emission as follows. The first is the quantum size effect proposed by Canham [36]. The second is the emission from the surface molecular species which coat the porous Si skeleton [37]. The third is the influence of the hydrogenated amorphous silicon [37]. The fourth is the emission from the radiative decay at surface/interface states, the characters of which are partly determined by nanocrystalline particles within the porous layer [37]. There are many studies on the visible emission, however, the origin of the visible emission has not yet been clarified because the oxidized surface structure of porous silicon is not homogeneous and cannot be adequately characterized. On the other hand, the surface of the OSI is not oxidized, therefore, the influence of the surface molecular species on the visible emission can be excluded. In this section, the size effects on the absorption and emission spectra from Si chain are discussed using OSI molecules.

The OSI prepared from the reaction of $SiCl_4$ has the size distribution. Fig. 12 shows the GPC elution curves of various molecular weight components obtained by fractional precipitation of *tert*-butyl-substituted OSI. The molecular weights M_w and the distributions M_w/M_n of fractionally precipitated OSI are summarized in Table 1. Although the molecular weight distributions of the highest M_w component (fraction 1) is not monodispersed, those of the other components are lower than 2. The structural changes of the OSI with increasing the M_w are investigated by far-IR spectra of the Si skeleton. Fig. 13 shows far-IR spectra of fractions 1, 3, and 7. There are three characteristic bands in the far-IR region although the intensity ratios are different from each other. The main band of the OSI with the lowest M_w (fraction 7) appears 519 cm^{-1} accompanying two weak bands at 439 and 400 cm^{-1}. With increasing the M_w, the

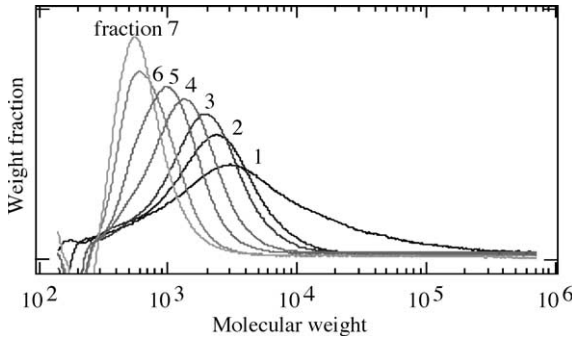

Fig. 12. GPC elusion curves of *tert*-butyl-substituted OSI. The molecular weights are determined using the THF eluent and monodispersed polystyrenes as the standards.

Table 1
Molecular weight and molecular weight distribution of *tert*-butyl-substituted OSI after fractional precipitation

Fraction	M_w	M_w/M_n
1	12 900	7.64
2	2550	1.91
3	2260	1.70
4	1440	1.41
5	1110	1.30
6	843	1.25
7	704	1.20

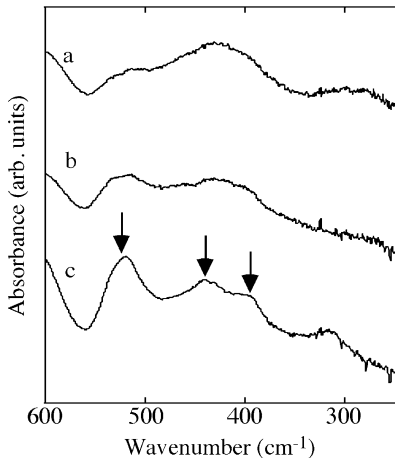

Fig. 13. Far-IR spectra of *tert*-butyl-substituted OSI. (a) fraction 1, (b) fraction 3, (c) fraction 7.

band around 519 cm^{-1} is lowered and intensities of the other two bands are increasing. These bands can be attributed to 6, 4, and 5-membered rings in the Si skeleton, respectively, by comparison to calculated spectra (Fig. 14). These spectra are obtained by semi-empirical MO calculations using MNDO method, where models consisting of Si and H atoms are employed to simplify the calculations. This result suggests the amorphous structure of the OSI consisting of various kinds of silicon rings.

Using the OSI with various M_w, the size effects on the absorption and emission spectra were investigated. Fig. 15 shows the Tauc plots of the absorption spectra of OSI and the optical band gap $E_{g,opt}$ obtained from the intercept of the tangential line of the Tauc plots. With increasing the molecular weight M_w, the $E_{g,opt}$ shifts to lower energy (Fig. 15 B). The emission spectra of OSI also show similar size dependence as shown in Fig. 16. The emission maximum shifts to longer wavelength, that is, lower energy, with increasing the molecular weight (Fig. 16). The emission maximum of the fraction 1 ($M_w = 12\,900$) is 528 nm, which is rather large compared to those of network polysilanes with the higher molecular weights [4–7]. Such a characteristic behavior of the OSI may be due to the Si skeleton consisting of four-coordinate Si atoms, that is, the three-dimensional σ-conjugation along the Si skeleton. In Fig. 17, the values of band gap E_g from the Tauc plots and those from the emission maxima are plotted against the diameter of Si core in comparison with the literature values for inorganic nanosilicons such as surface-oxidized silicon nanocrystal [38], microcrystalline Si:H [39], and ultrafine Si particles in a Si oxide matrix [40]. The size of the OSI was estimated from those of monodispersed polystyrenes which were used as standards in the size exclusion chromatography considering the composition of the organic side chain [32,41]. Littau et al. have reported the comparison of the sizes of surface-oxidized Si nanocrystals determined by transmission electron microscopic analysis and size exclusion chromatography and the good agreement between the two methods [38].

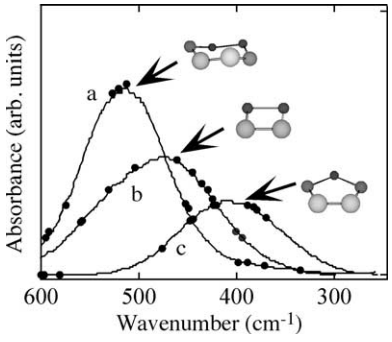

Fig. 14. Calculated spectra for model compound using MNDO method. (a) 6-membered ring, (b) 4-membered ring, (c) 4-membered ring.

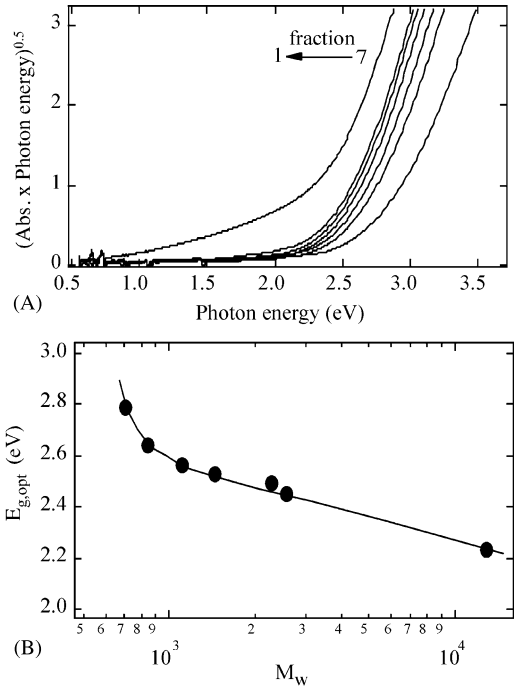

Fig. 15. Tauc plots of the absorption spectra of *tert*-butyl-substituted OSI (A) and the plots of the optical band gap versus molecular weight M_w (B).

The E_g values of organosilicon nanoclusters increase from 2.23 to 2.79 eV with decreasing the diameters of the Si core from 1.85 to 1.09 nm. The increase of the E_g can be explained by considering the quantum size effects in the optical properties. The sizes of the OSI are smaller

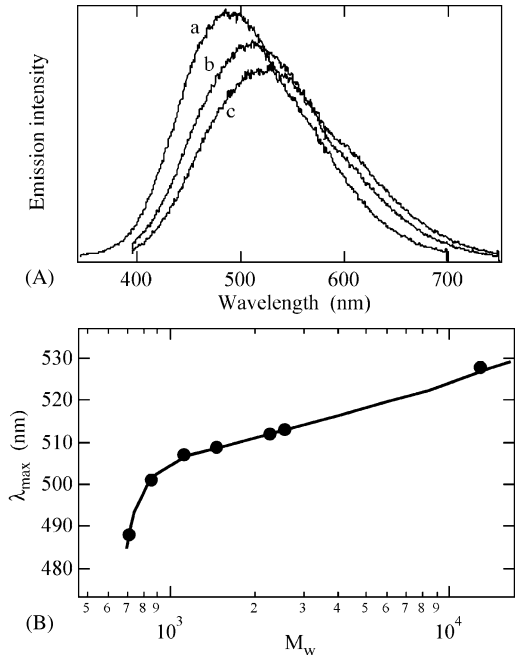

Fig. 16. Emission spectra of *tert*-butyl-substituted OSI (A) and the plots of the emission maximum λ_{max} versus molecular weight M_w (B). (a) Fraction 7, (b) fraction 3, (c) fraction 1.

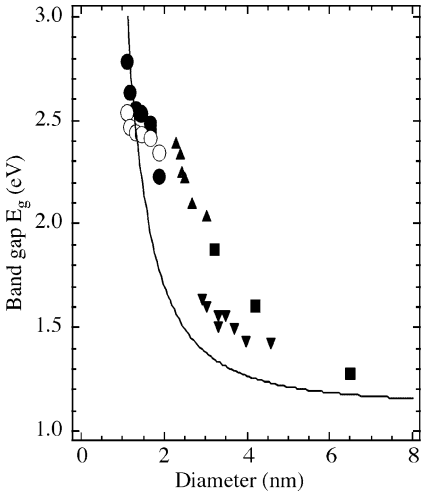

Fig. 17. Size dependence of the band gap Eg of silicons. (●) This work, Eg obtained from Tauc plots of absorption spectrum, (○) this work, Eg obtained from emission maximum, (—) this work; theoretical calculation for quantum dot, (■) [38], (▼) [40], (▲) [39].

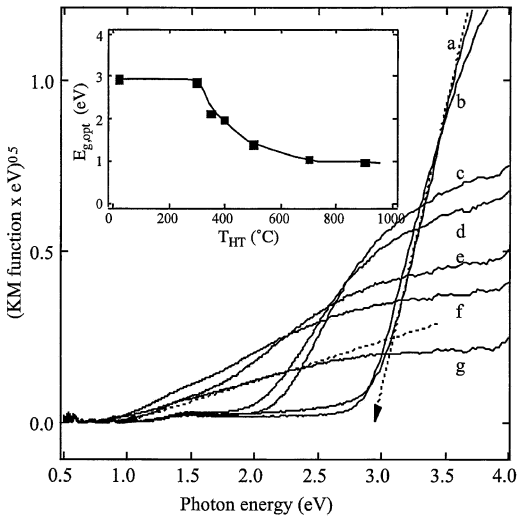

Fig. 18. Tauc plots of *n*-propyl-substituted OSI heat-treated at various temperatures in vacuo. (a) No heat treatment, (b) 300 °C, (c) 350 °C, (d) 400 °C, (e) 500 °C, (f) 700 °C, (g) 900 °C.

than those of inorganic nanosilicons and they supply the data for nanosilicons whose diameters are smaller than 2 nm. The continuous change of the E_g by quantum size effects is seen for organic and inorganic nanosilicons.

6. Materials beyond the border between organic and inorganic silicons

The OSI is a chemically synthesized three-dimensional silicon with a nanometer size and it can be handled in air and solvents because of the organic side chains around the Si nanocluster. The solubility of the OSI decreases with increasing the size, therefore, there is a limitation of the size synthesized chemically in solution. One of the purposes of this study is the material design and synthesis beyond the border between organic and inorganic materials. Polysilanes and inorganic nanosilicon such as a porous silicon are suitable models to discuss the properties of such materials. Next approach of this study is to prepare an inorganic silicon using an organic silicon as a precursor and to discuss the optical property in the interdisciplinary region.

Fig. 18 shows the spectral changes of *n*-propyl-substituted OSI films heat-treated in vacuo at various temperatures. The absorption edge shifts to lower energy with increasing heat treatment temperature. The optical band gaps $E_{g,opt}$ are determined by the Tauc plots and plotted against the heat treatment temperatures as shown in the insertion on Fig. 18. The $E_{g,opt}$ remarkably decreased around 400 °C, which corresponds to the thermogravimetric (T_g) curve of *n*-propyl-substituted OSI [26]. Such changes can be attributed to the reconstruction of the Si skeleton accompanying the elimination of organic side chain.

The emission spectra also show remarkable changes by heat treatment as shown in Fig. 19. The emission maximum of the *n*-propyl-substituted OSI film shifts to 650 nm by heat treatment at 350 °C, which also attributed to the change of the T_g curves. The emission maximum shifts to 700 nm by further heat treatment. These emission wavelengths correspond to those of porous silicon. These data demonstrate the continuous change of the emission properties from organic to inorganic silicon changing the structure of the Si skeleton.

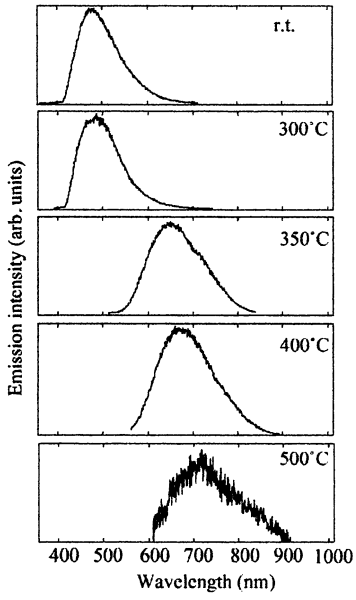

Fig. 19. Emission spectra of *n*-propyl-substituted OSI heat-treated at various temperatures in vacuo. Excitation wavelength: 380 nm (SHG) of Ti:sapphire laser.

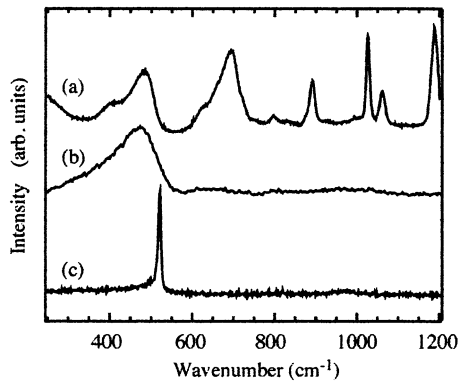

Fig. 20. Raman spectra of *n*-propyl-substituted OSI films without heat treatment (a), preheating at 400 °C for 30 min in vacuo, (b) and XeCl excimer laser-annealing by multistep irradiation at the energy densities of 200 mJ cm^{-2} (30 shots), 300 mJ cm^{-2} (30 shots), and 485 mJ cm^{-2} (30 shots).

The structural changes of the Si skeleton by heat treatment have been investigated by Raman spectroscopy. Fig. 20 (a) shows the Raman spectrum of the *n*-propyl-substituted OSI film without heat treatment, where the Raman band at 486 cm^{-1} is assigned to the transverse optical (TO)-phonon band of the Si–Si lattice and other bands above 600 cm^{-1} are assigned to the organic substituents. The Raman bands of the organic side chain disappear completely by heat treatment at 400 °C as shown in Fig. 20 (b) [26]. A broad band at 480 cm^{-1} is attributable to the *a*-Si structure. The Si skeleton of the heat-treated OSI is amorphous even by the heat treatment at 1000 °C if an electric furnace is employed. Recently, Watanabe et al. reported the crystallization of the Si skeleton of the OSI using XeCl excimer laser annealing [27]. The Raman spectrum of the OSI film after excimer laser annealing are shown in Fig. 20 (c), where the procedure of the multistep irradiation was employed: 200 mJ cm^{-2} (30 shots); 300 mJ cm^{-2} (30 shots); 485 mJ cm^{-2} (30 shots) after preheating at 400 °C. The narrow band at 520 cm^{-1} suggests the crystallization of the Si lattice. The morphological changes of the film before and after laser annealing were observed by scanning electron microscope (SEM). The SEM micrographs of laser-annealed film is observed after SECCO solution (49% HF: 0.15 mol dm^{-3} $K_2Cr_2O_7$ = 2:1, v/v) etching, where *a*-Si parts are selectively etched and crystalline silicon (*c*-Si) parts remain. Without laser annealing, the SEM micrograph of the OSI film heat-treated at 400 °C shows a homogeneous surface. The roughness of the film was estimated to be less than 2 nm by atomic force microscope (AFM) measurements. Such smoothness of the film surface is due to the evaporation of the organic moieties under the melting condition of the OSI film by heat treatment. On the other hand, the formation of grains was observed after laser annealing as shown in Fig. 21, which demonstrates the formation of nanoparticles

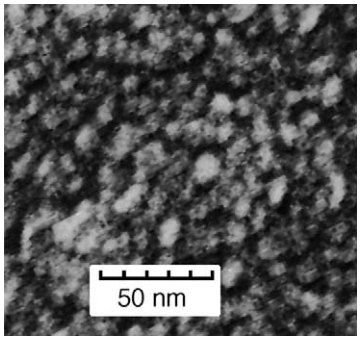

Fig. 21. SEM micrographs of laser-annealed films. Multistep irradiation: 200 mJ cm^{-2} (30 shots); 300 mJ cm^{-2} (30 shots); 485 mJ cm^{-2} (30 shots) after preheating at 400 °C.

approximately 10 nm in size by multistep laser irradiation of OSI.

7. Experimental

7.1. Materials

The OSI was obtained by the reaction of silicon tetrachloride using Mg metal in THF at 10 °C under ultrasonic field and the replacement of the remaining Si–Cl group with alkyl group (*n*-propyl or *tert*-butyl group). After the reaction was completed, the mixture was poured into methanol and the OSI was obtained as a precipitate. To remove the oxidized products, the precipitates were purified by column chromatography using silica gel. The details of the procedures are described elsewhere [13,14,27,32]. The films of polysilanes were prepared by spin coating on a quartz substrate from toluene solutions. The heat treatment of the OSI film was carried out using an electric furnace under vacuum evacuated to less than 10^{-4} Pa. The crystallization of the organosilicon nanocluster film was carried out by XeCl excimer annealing. After preheating of the organosilicon nanocluster film at 400 °C for 30 min in vacuo, the thickness of the film was reduced to approximately 50 nm, and the 308 nm laser pulse of an XeCl laser was irradiated under an argon atmosphere.

7.2. Measurement

The time-resolved emission spectra were measured using an argon ion laser (Spectra-Physics, BeamLok 2060-10-SA) pumped Ti:sapphire laser (Spectra-Physics, Tsunami 3950-L2S) with a pulse selector (Spectra-Physics, Model 3980), a harmonic generator (GWU-23PS), and a streak scope (HAMAMATSU, C4334-01, sweep repetition rate 2 MHz). In the measurements, by setting a threshold level for the A/D converted CCD camera signal, the photoelectron image can be clearly separated from the noise. The system enables photon

counting measurements at simultaneous multiple wavelengths. The typical instrument response time for this apparatus is 20 ps (fwhm) and time resolution of the detection within 5 ps can be obtained by using a deconvolution technique.

The molecular orbital calculations of a polysilane dendrimer were carried out using the CAChe system (Sony Tektronics). The optimized geometries of the polysilane dendrimer in the ground and excited state were calculated by the PM3 method using the semi-empirical MOPAC package.

The IR and far-infrared absorption spectra were measured using a JEOL100 FT-IR spectrophotometer. The Far-IR spectra were measured using a sample prepared by dispersing a polysilane into a paraffin matrix and pasting it on a polyethylene. Raman spectra were measured by a micro-Raman apparatus equipped with a liquid nitrogen-cooled charge-coupled device detector. All samples were excited with the 488 nm line from an argon ion laser.

8. Conclusion

The advantage of organic silicons is the flexibility in the molecular design and synthesis. Polysilanes with various Si skeletons provide a model to study the effect of Si dimensionality on the optical properties, where linear polysilane, network polysilane, and OSI can be considered as pseudo one-, two-, and three-dimensional silicons, respectively. The emissions of polysilanes with branching Si chain are characterized by the dual emission in the UV and visible regions and the large Stokes shift between the absorption and emission spectra. The localized excited state induced by the distortion of the Si–Si chain around the branching point was suggested. In the excited state, the distortion is focused on the branching point, and the σ-conjugation is discontinued at the branching point by the formation of the localized excited state having a triangular structure. Such a specific behavior in the excited state is due to the flexibility of the Si–Si chain and the σ-conjugation which is sensitive to the conformation of the Si–Si chain. In other words, the emission from the branching Si chain needs the conformational change in the excited state. The organic silicons having a flexible structure are usually luminescent, whereas *c*-Si having a rigid structure shows no emission. Porous silicon has a large surface where the Si chain is terminated by oxygen. Around the surface, the flexibility of the Si lattice must be induced by the Si–O–Si chain in comparison with the crystalline silicon surface. The visible emission of porous silicon may be attributed to the emission from the distorted excited state near the oxidized surface.

Another factor that affects the optical properties of silicon is the quantum size effect. Using the OSI with various M_w, the size effects on the absorption and emission spectra were investigated. The sizes of the OSI are smaller than those of inorganic nanosilicons and they supply the data for nanosilicons whose diameters are smaller than 2 nm. The continuous change of the E_g by quantum size effects is seen for organic and inorganic nanosilicons.

Acknowledgements

This work was supported by Grants-in-Aid for Scientific Research (Nos. 1155900 and 13650942) from the Ministry of Education, Culture, Sports, Science, and Technology.

References

[1] R.D. Miller, J. Michl, Chem. Rev. 89 (1989) 1359.
[2] N. Matsumoto, in: W. Bergholtz, K. Sumino (Eds.), Semiconductor Silicon/1994, Electrochem. Soc., Pennington, 1994.
[3] W.L. Wilson, T.W. Weidman, J. Phys. Chem. 95 (1991) 4568.
[4] A. Watanabe, H. Miike, Y. Tsutsumi, M. Matsuda, Macromolecules 26 (1993) 2111.
[5] P.A. Bianconi, T.W. Weidman, J. Am. Chem. Soc. 10 (1988) 2342.
[6] P.A. Bianconi, F.C. Schilling, T.W. Weidman, Macromolecules 22 (1989) 1697.
[7] K. Furukawa, M. Fujino, N. Matsumoto, Macromolecules 23 (1990) 3423.
[8] A. Watanabe, M. Matsuda, Chem. Lett. (1991) 1101.
[9] A. Watanabe, M. Matsuda, Y. Yoshida, S. Tagawa, ACS Symp. Ser. 579 (1994) 408.
[10] A. Watanabe, O. Ito, M. Matsuda, M. Suezawa, K. Sumino, Jpn. J. Appl. Phys. 33 (1994) 4133.
[11] H. Matsumoto, H. Miyamoto, N. Kojima, Y. Nagai, J. Chem. Soc. Chem. Commun. (1987) 1316.
[12] A. Watanabe, M. Fujitsuka, O. Ito, T. Miwa, Jpn. J. Appl. Phys. 36 (1997) L1265.
[13] A. Watanabe, M. Fujitsuka, O. Ito, T. Miwa, Mol. Cryst. Liq. Cryst. 316 (1998) 363.
[14] A. Watanabe, M. Fujitsuka, O. Ito, Thin Solid Film 354 (1999) 13.
[15] J.B. Lambert, J.L. Pflug, C.L. Stern, Angew. Chem. Int. Ed. Engl. 34 (1995) 98.
[16] A. Sekiguchi, M. Nanjo, C. Kabuto, H. Sakurai, J. Am. Chem. Soc. 117 (1995) 4195.
[17] H. Suzuki, Y. Kimata, S. Satoh, A. Kuriyama, Chem. Lett. (1995) 293.
[18] L.T. Canham, Appl. Phys. Lett. 57 (1990) 1046.
[19] J.L. Heinrich, C.L. Curtis, G.M. Gredo, K.L. Kavanagh, M.J. Sailor, Science 255 (1992) 66.
[20] J.C. Vial, J. Derrien, Porous Silicon Science and Technology, Springer-Verlag, Berlin, 1995.
[21] H. Kamimura, Y. Kanemitsu, M. Kondo, K. Takeda, Light Emission from Novel Silicon Materials, The Physical Society of Japan, Tokyo, 1994, p. 1994.
[22] R.A. Street, D.K. Biegelsen, R.L. Weisfield, Phys. Rev. B30 (1984) 5861.

[23] M.S. Brandt, H.D. Fuchs, M. Stutzmann, J. Weber, M. Cardona, Solid State Commun. 81 (1992) 307.
[24] S.M. Probes, O.J. Glembock, V.M. Bermudes, R. Kaplan, Phys. Rev. B45 (1992) 13788.
[25] M. Fujino, H. Isaka, J. Chem. Soc. Chem. Commun. (1989) 466.
[26] A. Watanabe, M. Unno, F. Hojo, T. Miwa, Jpn. J. Appl. Phys. 39 (2000) L961.
[27] A. Watanabe, F. Hojo, T. Miwa, M. Wakagi, Jpn. J. Appl. Phys. 41 (2002) L378.
[28] J.B. Lambert, J.L. Pflug, J.M. Denari, Organometallics 15 (1996) 615.
[29] J.B. Lambert, J.L. Pflug, C.L. Stern, Organometallics 17 (1998) 4904.
[30] M. Nanjo, A. Sekiguchi, Organometallics 17 (1998) 492.
[31] M. Nanjo, T. Sunaga, A. Sekiguchi, E. Horn, Inorg. Chem. Commun. 2 (1999) 203.
[32] A. Watanabe, T. Sato, M. Matsuda, Jpn. J. Appl. Phys. 40 (2001) 6457.
[33] M. Fujiki, Chem. Phys. Lett. 198 (1992) 177.
[34] A. Watanabe, M. Nanjo, T. Sunaga, A. Sekiguchi, J. Phys. Chem. A 105 (2001) 6436.
[35] A. Watanabe, Y. Tsutsumi, M. Matsuda, Synthetic Metals 74 (1995) 191.
[36] L.T. Canham, Phys. Stat. Sol. 190 (1995) 9.
[37] B. Hamilton, Semicond. Sci. Technol. 10 (1995) 1187.
[38] K.A. Littau, P.J. Szajowski, A.R. Muller, A.R. Kortan, L.E. Brus, J. Phys. Chem. 97 (1993) 1224.
[39] S. Furukawa, T. Miyasato, Phys. Rev. B 38 (1988) 5726.
[40] T. Takagi, H. Ogawa, Y. Yamazaki, A. Ishizaki, T. Nakagiri, Appl. Phys. Lett. 56 (1990) 2379.
[41] M. Kurata, Y. Tsunashima, M. Iwama, K. Kamada, in: J. Brandrup, E.H. Immergut (Eds.), Polymer Handbook, 2nd ed (Chapter IV), John Wiley & Sons, New York, 1975, p. 41 (Chapter IV).